

The amplitudons of dynamical stable binary cubic crystals for hot-electron cooling in BaTe, CdTe, SrTe and SnTe for enhanced photo voltaic effect.

T.E.Ada^{1,*}, L.D. Deja², D.A. Adem³, and K.N. Nigussa^{2,*}

¹Department of Physics, Dilla University, P.O. Box 419, Dilla, Ethiopia

^{2,3}Department of Physics, Addis Ababa University, P.O. Box 1176, Addis Ababa, Ethiopia

³Department of Physics, Wolkite University, P.O. Box 07, Wolkite, Ethiopia

*corresponding.kenate.nemera@aau.edu.et

*corresponding.tewodros.eyob@aau.edu.et

ABSTRACT

Dynamical properties of materials determined using force constant expansions in the HIPHIVE package and density functional theory as implemented in the Gpaw code. Thermal conductivity of alkaline earth tellurides was determined, and the narrower width between amplitudons and electrical modes exhibited supersonic cooling and heat transportation, and our findings are in perfect agreement with experimental research. When compared to the other binary crystals, BaTe appears to offer the dual advantage of prolonged photon lifetime at normal temperature as well as a speedier thermo-electric converter due to the tiny gap between amplitudons and electric modes.

Introduction

Thermoelectric materials have attracted significant research in recent years due to their promise in energy applications such as converting waste heat into power and replacing mechanical cooling systems with more environmentally friendly thermoelectric devices. For decades, in fact, the goal has been to improve the energy conversion efficiency, which is characterized by the dimensionless figure of merit, zT , which is defined as the ratio of the electronic power factor and the thermal conductivity of the thermoelectric material, and fixed to only $zT = 1.0$. However, a surprising 40% increase in zT value from 1.0 to 1.4 was accomplished by using a ball milling and hot pressing procedure on an ingot^{1,2}. A further 50% improvement has been made to that of Bi_2Te_3 ingot materials accounting for $zT = 1.56$ at 300 K³. Because anharmonic lattice dynamics necessitate both high electronic power factors and low thermal conductivities⁴, increasing the figure of merit is to reduce the phonon contribution to thermal transport while maintaining electrical conductivity unaltered, either by a high Seebeck coefficient or a low thermal conductivity⁵. Identifying a phonon blocking mechanism is thus beneficial.

One example of how defected crystals can affect a material's electrical properties is by scattering or localizing electrons, which in turn decreases the power factor. Another way that lattice disorder can impact a material is by introducing loosely bound rattling atoms into crystals with complex unit cells, which can limit the flow of heat and make thermoelectric conversion less efficient^{6,7}.

It is evident that the presence of two or more mutually incompatible elements of translational symmetry implies the presence of continuously accumulated phase shifts, causing an acoustic-like excitation coming from the incommensurate modulation consisting of two modes amplitudon (optic-phonon-like) and phason (acoustic phonon-like). The temperature dependence of the wave vector near commensurate phase forms solitons, which are completely analogous to phonons in a regular atomic lattice; however, the soliton lattice is faster than the crystal lattice. Thus, phasons travel faster than acoustic phonons, reduce domain wall energy, and favor incommensurate phases^{8,9}.

In what is now known as the FPU recurrent phenomena, researchers discovered that energy traveling between degrees of freedom remained unevenly distributed at any scale. Some complicated nonlinear systems can be chaotic or extremely complex while still being predicted to be ergodic. However, some nonlinear systems, such as the FPU simulation, create coherent nonlinear structures and traveling waves.

For instance, a soliton is a solitary traveling wave solution that is the quintessential coherent structure encountered in many macroscopic nonlinear systems. In addition to the previously described efforts on nonlinear traveling waves in one dimensional lattices, Mathew *et al*¹⁰ have reported three-dimensional crystal lattices that allow anharmonicity-driven intrinsic localized modes (ILMs), which are stationary vibrations limited to only a few atoms.

Localization and related changes in the lattice dynamics in a PbSe crystal using inelastic neutron and x-ray scattering, on the other hand, show that localization occurs at close to predicted temperatures but involves more spectral weight than expected and drives unanticipated changes in the lattice dynamics, including an unexpected sharpening of the longitudinal acoustic (LA) phonon at high temperatures. Instead of localizing with a fraction of the intensity of normal phonons¹¹, the entire spectral weight of a significant portion of the transverse optic phonon immediately acquires flat dispersion (zero group velocity) and appears frequency fragmented.

The anharmonic dynamics transition can be seen in the optic phonon's localization (flattening) and fragmentation^{12,13}. This transition has also been found as a minor kink in the thermal diffusivity data, which is analogous to ILM ordering in NaI.

The discovery of in-band localization in a PbSe crystal not only broadens the domain of anharmonic localization, but also has crucial implications for the low thermal conductivity required for thermoelectric performance. One can see that the reorganization of spectral characteristics caused by localization profoundly alters the phase space for scattering, which explains the sharpening of the LA phonon. These findings demonstrate that nonlinear physics beyond standard harmonic perturbations can play a significant role in influencing vibrational transport.

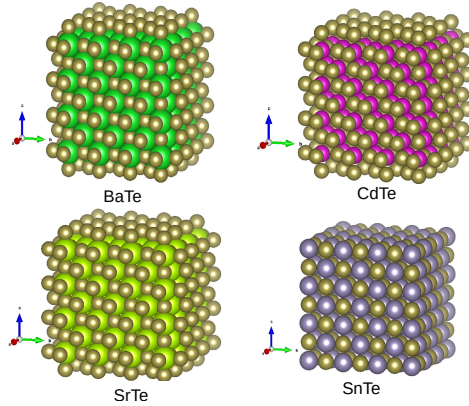


Figure 1. Cubic crystal structures of BaTe, SrTe, and SnTe were substituted on the prototype CdTe system to highlight the incommensurate structure considerations.

CdTe has been identified as one of the most promising absorber materials for thin-film solar cells. As a result, continued research activities in CdTe-based photovoltaics remain highly appealing. According to one claim, substituting or doping of CdTe-material optimizes carrier collection¹⁴⁻¹⁶, resulting in a considerable improvement in CdTe solar-cell performance.

Here we look at the incommensurate modulation originates due to Ba, Sr and Sn substituted in CdTe crystal system. CdTe is Halite, Rock Salt structured and crystallizes in the cubic space group. The corner-sharing octahedral are not tilted (See Fig. 1).

1 Methodology

In crystals, it is assumed that atoms move around their equilibrium position, thus, the potential surface can be expanded in a Taylor series with respect to the atomic displacements, \mathbf{u} relative to a set of reference positions, R_0 .

$$\begin{aligned}
 V = & \Phi_0 + \sum_i \sum_a \Phi_i^\alpha u_i^\alpha + \frac{1}{2!} \sum_{ij} \sum_{\alpha\beta} \Phi_{ij}^{\alpha\beta} u_i^\alpha u_j^\beta \\
 & + \frac{1}{3!} \sum_{ijk} \sum_{\alpha\beta\gamma} \Phi_{ijk}^{\alpha\beta\gamma} u_i^\alpha u_j^\beta u_k^\gamma + \frac{1}{4!} \sum_{ijkl} \sum_{\alpha\beta\gamma\eta} \Phi_{ijkl}^{\alpha\beta\gamma\eta} u_i^\alpha u_j^\beta u_k^\gamma u_l^\eta + \dots
 \end{aligned} \tag{1}$$

Where Φ is crystal potential, while Latin and Greek indices enumerate atoms and Cartesian coordinates, respectively. From eq. 1 the coefficients of series expansions, Φ_0 , Φ_i^α , $\Phi_{ij}^{\alpha\beta}$, and $\Phi_{ijk}^{\alpha\beta\gamma}$ are the zeroth, first, second, and third order force constants, respectively. Atomic vibration is solved with second order terms as harmonic approximation with small displacement at constant volume. Thus, the force acting on atom i along direction α is given by

$$\begin{aligned}
 F_i^\alpha = & -\frac{\partial V}{\partial u_i^\alpha} = -\sum_j \sum_\beta \Phi_{ij}^{\alpha\beta} u_j^\beta - \frac{1}{2!} \sum_{jk} \sum_{\beta\gamma} \Phi_{ijk}^{\alpha\beta\gamma} u_j^\beta u_k^\gamma \\
 & - \frac{1}{3!} \sum_{jkl} \sum_{\beta\gamma\eta} \Phi_{ijkl}^{\alpha\beta\gamma\eta} u_j^\beta u_k^\gamma u_l^\eta + \dots
 \end{aligned} \tag{2}$$

Applying derivative operator to a force $F_i = -\frac{\partial\Phi}{\partial u_i}$, one come up with second order force constants,

$$\frac{\partial^2\Phi}{\partial u_\alpha\partial u_i} = -\frac{\partial F_i}{\partial u_\alpha} \quad (3)$$

Dynamical property of atoms in the harmonic approximation is obtained by solving eigenvalue problem of dynamical matrix, $D(q)$.

$$\sum D(q)e_{qj} = \omega^2 e_{qj} \quad (4)$$

Solving Newton's equations of motion requires solving for the eigenvalues of the dynamical matrix, the eigenvalues of the dynamical matrix are the squared frequencies. Note that, each frequency corresponds to a phonon mode, e_{qj} dynamical matrix is a function of the wave vector, q with associated j dimensional Cartesian axes. Since $D(q)$ is an Hermitian matrix, its eigenvalues, ω_{qj}^2 , are real. Phononic characteristics could indicate dynamical stability of crystal structure, for instance, phonons with real & positive frequency indicates that the system is stable, however, imaginary frequency or negative eigenvalue show dynamical instability of a system which means the corrective atomic displacement required or imaginary mode give a clue to study displace phase transition¹⁷. The phonon density of states is calculated as

$$g(\omega) = \frac{1}{N} \delta(\omega - \omega_{qj}) \quad (5)$$

Where N is the number of unit cells in crystal, phonon mode at unique frequency over Brillouin zone plotted as as shown in Fig. (5) the band structure explains acoustic modes damped gradually to Γ -center which relates to lower thermal conductivity, further decrement in thermal conductivity expected due to presence of many phonon modes, the energy of phonon system determined as

$$E = \sum_{qj} \hbar\omega_{qj} \left[\frac{1}{2} + \frac{1}{\exp(\hbar\omega_{qj}/k_B T) - 1} \right] \quad (6)$$

Where T , k_B , and \hbar are the temperature, the Boltzmann constant, and the reduced Plank constant, respectively. Using the thermodynamic relations, a number of thermal properties, such as constant volume heat capacity, C_V

$$C_V = \sum_{qj} C_{qj} = \sum_{qj} k_B \left(\frac{\hbar\omega_{qj}}{k_B T} \right)^2 \frac{\exp(\hbar\omega_{qj}/k_B T)}{[\exp(\hbar\omega_{qj}/k_B T) - 1]^2}, \quad (7)$$

Helmholtz free energy F ,

$$F = \frac{1}{2} \sum_{qj} \hbar\omega_{qj} + k_B T \sum_{qj} \ln[1 - \exp(-\hbar\omega_{qj}/k_B T)], \quad (8)$$

and entropy S ,

$$S = \frac{1}{2T} \sum_{qj} \hbar\omega_{qj} \coth[\hbar\omega_{qj}/2k_B T] - k_B \sum_{qj} \ln[2\sinh(\hbar\omega_{qj}/2k_B T)] \quad (9)$$

The diagonal components of the thermal conductivity tensor are where $V_{\alpha qj}$ is the group velocity of the mode, q_j and $\tau_{\alpha q}$ is the mode lifetime for transport in direction α , C_q is the mode heat capacity, and V is volume. As illustrated in Fig.(6), thermal conductivity is supposed to be insensitive to temperature changes & computed as,

$$\kappa_{\alpha\alpha} = \frac{1}{V} \sum_{qj} C_{qj} V_{\alpha qj} \tau_{\alpha qj} \quad (10)$$

Phonon calculation¹⁸ explains thermal properties, mechanical properties, phase transition, and superconductivity. Thermodynamic variables at constant volume is transformed to those at constant pressure.

$$G(T, P) = \min_V [F(T; V) + PV] \quad (11)$$

Gibbs free energy $G(T,P)$ at given temperature, T and pressure, P is obtained from Helmholtz free energy $F(T;V)$ through the transformation. Phonon lifetime is crucial in search of thermoelectric materials, transistors, and heat management systems since it could explain how long it takes phonon mode vibrations to dissipate¹⁹. Peaks in Fig. (4) represent key phonon modes that contribute to overall phonon life time throughout frequency, which corresponds to temperature.

Here, we investigate a BaTe, SrTe, SnTe cubic dimmer from the space group $Fm-3m$ (International Tables of Crystallography number 225). Random displacements were applied to perfect supercells with up to 216 atoms (equal to $3 \times 3 \times 3$ unit cells) to generate input configurations. The average displacement amplitudes for these configurations were around 0.0098, resulting in average forces of around 230 meV per angstrom and maximum forces of around 0.6 eV per angstrom. DFT computations were used to generate reference forces, which were obtained using the projector augmented wave method^{20–22} as implemented in GPAW code²³ and the vdW-DF-cx method²⁴, which combines semi-local exchange with nonlocal correlation. The Brillouin zone was sampled with Monkhorst Pack k-point grids, which are equivalent to a $2 \times 2 \times 2$ mesh relative to the primitive cell. The plane-wave energy cutoff was set to 333 eV, the forces were evaluated using a finer grid, and the reciprocal projection scheme was used throughout the calculation.

Fig.(5) depicts the phonon dispersion produced using hiphive²⁵ with all invariant constraints imposed. The lowermost transverse acoustic branch clearly demonstrates quadratic dispersion in this case. If the rotational sum rules are deactivated, the dispersion is almost unchanged except for the appearance of a small imaginary pocket in the immediate vicinity of the Brillouin center, and thus does not yield a quadratic dispersion, but small errors can have a significant effect whenever the acoustic modes contribute significantly to a property, such as thermal conductivity. The thermal conductivity was calculated using the phono3py code in the setting of phonon Boltzmann transport theory in the relaxation time approximation²⁶. The Brillouin integration was performed using the tetrahedron method and a $13 \times 13 \times 13$ q-point mesh. Only phonon-phonon scattering was regarded as a rate-limiting process for clarity. Reference computations were performed on pairings with distances up to 6.0 angstrom.

For all systems, a fourth-order FCP was generated with cutoff radii of 6.0, 5.0, and 5.0 angstrom for second, third, and fourth-order terms, respectively, corresponding to 216 clusters in the unit cell. The associated cluster space included 34 distinct orbits (6, 8, and 20 for second-, third-, and fourth-order, respectively), with interactions up to the fourth nearest neighbor for the pairings, resulting in 194 free parameters.

Training data consisted of five structures with 216 atoms ($3 \times 3 \times 3$ conventional unit cells) for a total of 3240 force components. The structures were created by using displacements taken at random from a normal distribution and tweaked to avoid inter-atomic distances shorter than 2.3 angstrom. The average atomic displacement as a result was around 0.13 angstrom. The reference forces were calculated using a grid-based augmented plane wave implemented in the Gpaw code. Because the system is highly over determined, the model parameters were trained using traditional least-squares fitting.

2 Results and discussion

The optical photoabsorption spectrum and nonlinear effects can be estimated using time-dependent external perturbation, and interactions inside a material can be investigated by linearly combining atomic orbitals. As demonstrated in Fig. (4), the number of phonon modes at 0.5THz frequency is substantially more than the number of modes in CdTe, SrTe, and SnTe, respectively.

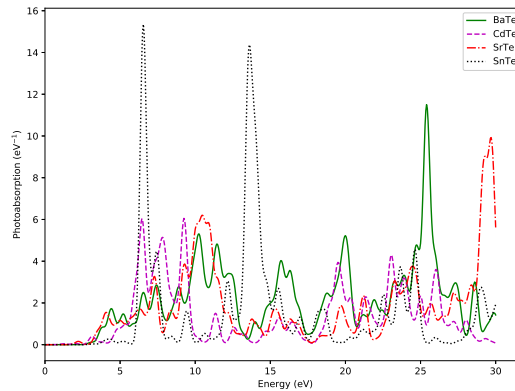


Figure 2. The photo absorption spectrum of the $\{Ba, Cd, Sr, \& Sn\}Te$ systems along z-axis for 30fs of time step and at kick strength of $1e^{-3}$ with grid parameter, $h = 0.3$, vacuum set to 6.0 with LCAO basis set assumed for constituent atom.

Although each constituent atom contributes positive real eigenvalued phonon modes, overall density reveals that instable modes exist for unknown reasons in the entire system as viewed in Fig. (3). If it were a clean perturbed system, it would have the optimum optical gap depicted in Fig. (2).

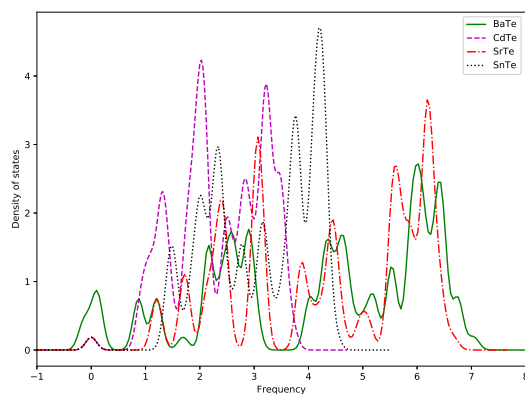


Figure 3. Density of states that contribute most to the lattice vibration of {Ba,Cd,Sr, & Sn}Te systems. For the interpretations of the references to color in this plot legend, the reader is referred to the web-version.

Despite the fact that Barium modes are more prevalent at lower frequencies and contribute higher proportion to the total phonon life time at room temperature, however, as temperatures rise Ba and Te modes doing not much in thermal cooling processes. Tellurium and Cadmium each have their own specific point where they separate in lesser proportions, and boost the phonon life. When Strontium and Tellurium were alloyed, their trends looks the same, but the phonon life time contribution the list on the scale as compared to rest of systems. Tin alloyed with Tellurium, on the other hand, has a much better than SrTe; nevertheless, at higher frequencies, both Tin and Tellurium mutually contribute to the phonon life time, as seen in Fig. (4).

Modes that oscillate in the same direction add up to optical modes in a spring model, but modes that oscillate against each other add up to acoustic modes. Surprisingly, as shown on left of Fig. (5), we have modes that execute the functions of optical and acoustic modes with improved cooling speed. Because the gap between amplitudon and electrical modes is narrow along the wave vector path, $K - \Gamma$, BaTe, and SrTe display excellent electrical and thermal conductivity. CdTe and SnTe, on the other hand, have a broad gap and no sharp modulation amplitude, making both forms of conductivity difficult. A narrower gap has a higher group velocity than a wider gap, as illustrated on the right of Fig. (5).

In thermoelectrics, thermal conductivity is the sum of electron-holes carrying heat (κ_e) and phonons passing through the lattice (κ_L). As a result, the thermoelectric figure of merit can be optimized by increasing electrical conductivity while decreasing thermal conductivity, alkaline earth tellurides are frequently employed as thermal conductivity moderators, increasing BaTe concentration reduces thermal conductivity of material in range [0, 2] as stated in Ref.^{27,28}, which corresponds with our study as shown in Fig. (6).

The results in Ref.²⁹ highlight experimentally determined pure CdTe thermal conductivity as 0.46 W/m.K, which is identical to our result, 0.42 W/m.K, and CdTe thermal conductivity shows a decrease over temperature range. Similarly, in Ref.³⁰, the minimal lattice thermal conductivity for SnTe is 0.81 W/m.K, whereas our result is 0.82 W/m.K. With the exception of SrTe, which has a thermal conductivity of 8.75 W/m.K, comparably alkaline earth tellurides have a low thermal conductivity.

3 Conclusion

Here we investigate in-band localization in BaTe, CdTe, SrTe and SnTe. We studied several modes with group velocity ranging from sound speed to super sonic speed. Our findings explain the sharpening of longitudinal acoustic phonon modes. It appears that heavier weighted Ba and Sr alloyed with tellurium have a much faster cooling nature due to sharp acoustic phonon modes. However, Cd and Sn seem to cool down just after a few nonlinear fluctuations. These findings demonstrate that it is possible to influence vibrational transport by doping heavy alkaline earth metal, which in turn allows for easier transportation of heat.

Disclosure statement

The authors declare that there is no conflict of interest.

4 Data Availability Statement

The data that support the findings of this study are available upon reasonable request from the authors.

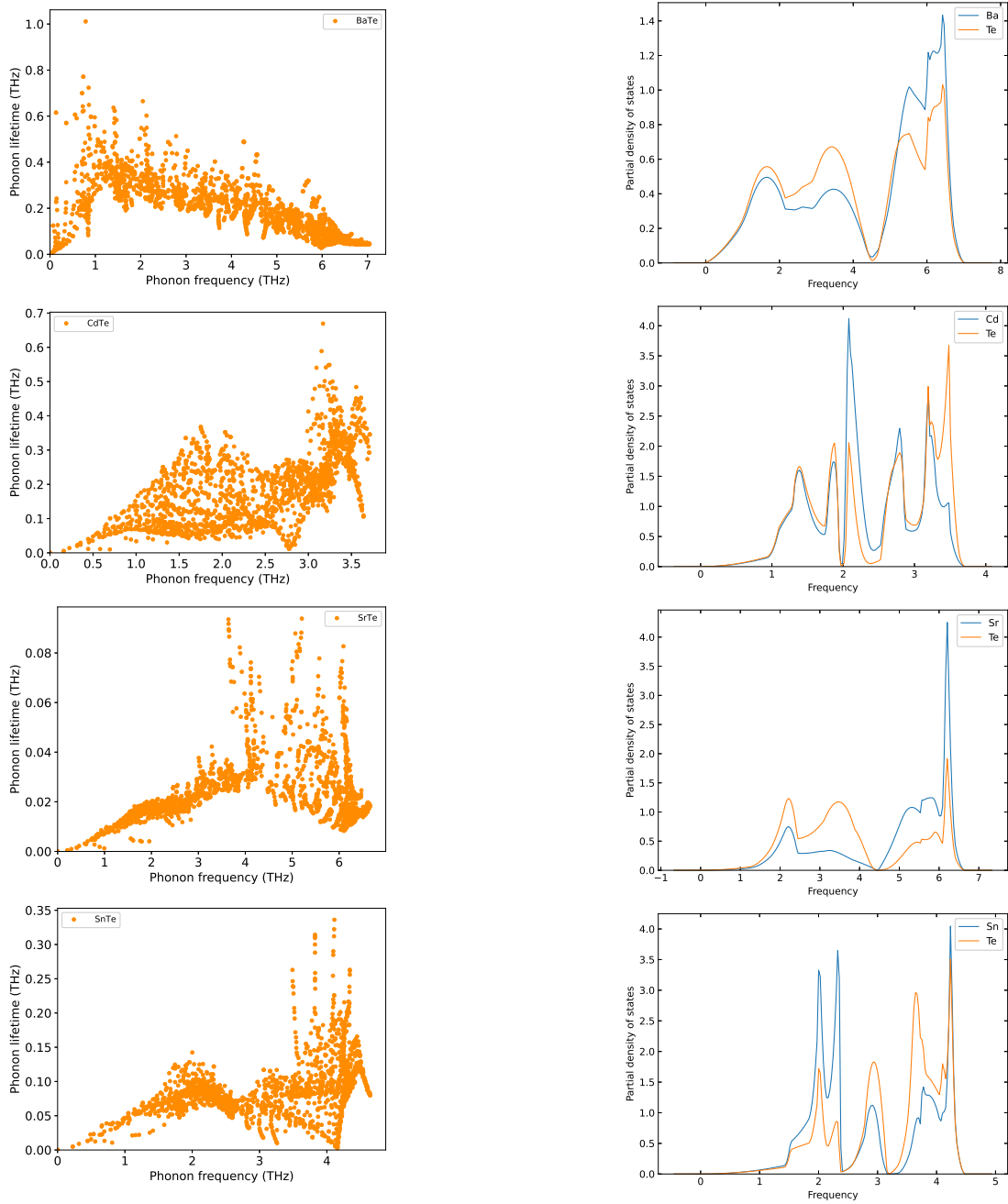


Figure 4. Phonon lifetime and Partial density of states of a) Phonon lifetime's scattered points (left side). b) Constituent contributor to total phonon density of States (right side). Color online. Phonon lifetimes corresponds to respective participant element of partial mode density as a function of frequency of BaTe, CdTe, SrTe, and SnTe, respectively.

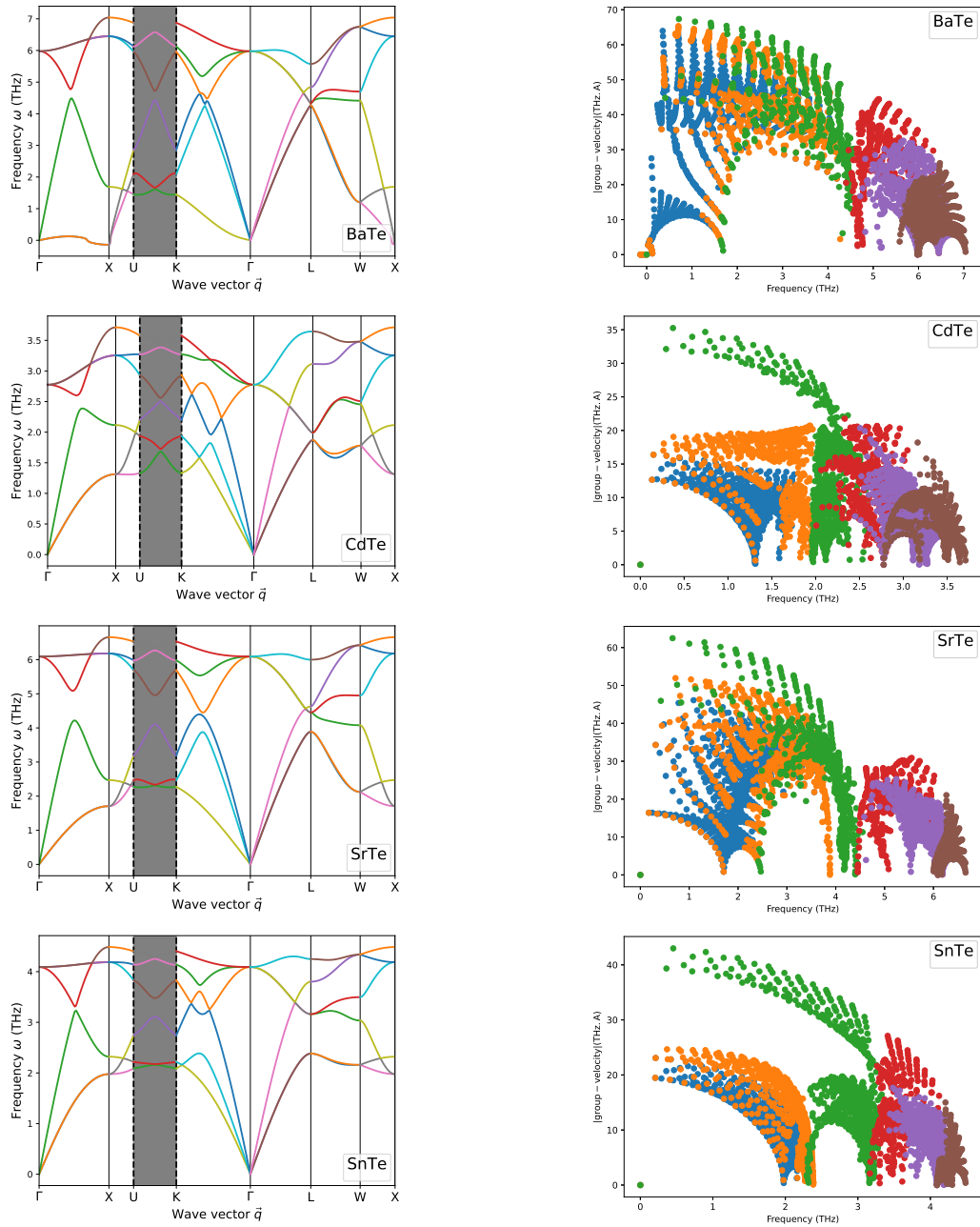


Figure 5. Phonon band structure and group velocities of a) Phonon dispersion (left side). b) Phonon group velocities (right side). Color online. Phonon dispersion curves in all colors, corresponds to similar color in group velocities as a function of frequency of different phonon modes for BaTe, CdTe, SrTe and SnTe, respectively.

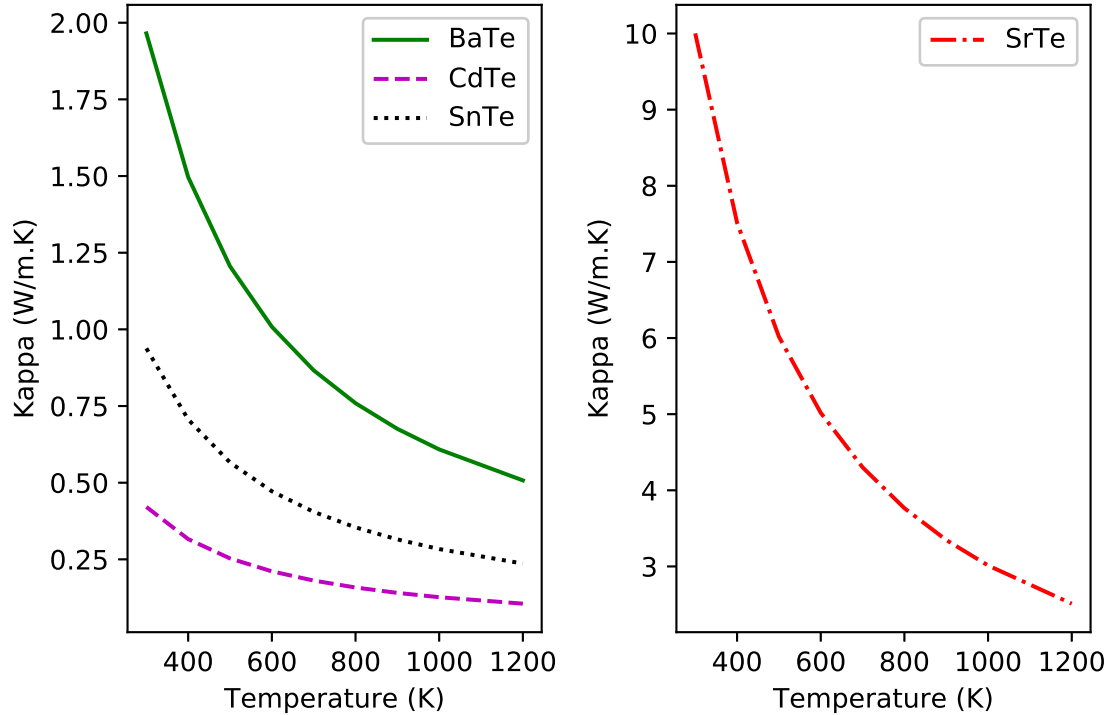


Figure 6. Calculated lattice thermal conductivity of {Ba, Cd, & Sr}Te systems against temperature plot (Left), and relatively scaled SrTe dimmer on (Right).

5 Acknowledgements

We are grateful to the Ministry of Education of Ethiopia for financial support. The authors also acknowledge the International Science Program, Uppsala University, Sweden, for providing computer facilities for research at the Department of Physics. The office of VPRTT of Addis Ababa university is also warmly appreciated for supporting this research under a grant number AR/053/2021.

References

1. Poudel, B. *et al.* High-thermoelectric performance of nanostructured bismuth antimony telluride bulk alloys. *Science* **320** (2008).
2. Wood, C. Materials for thermoelectric energy conversion. *Reports on Prog. Phys.* **51** (1988).
3. Xie, W., Tang, X., Yan, Y., Zhang, Q. & Tritt, T. M. Unique nanostructures and enhanced thermoelectric performance of melt-spun bisbte alloys. *Appl. Phys. Lett.* **94** (2009).
4. Nolas, G. S., Morelli, D. T. & Tritt, T. M. Skutterudites: A phonon-glass-electron crystal approach to advanced thermoelectric energy conversion applications. *Annu. Rev. Mater. Sci.* **29** (1999).
5. Delaire, J., O. and Ma *et al.* Giant anharmonic phonon scattering in pbte. *Nat. Mater.* **10** (2011).
6. Chen, Z. *et al.* Vacancy-induced dislocations within grains for high-performance pbse thermoelectrics. *Nat. Commun.* **8** (2017).
7. Manley, M. E. *et al.* Supersonic propagation of lattice energy by phasons in fresnoite. *Nat. Commun.* **9** (2018).
8. Bak, P. & von Boehm, J. Ising model with solitons, phasons, and the devil's staircase. *Phys. Rev. B* **21** (1980).
9. Quilichini, M. & Currat, R. Neutron evidence for an overdamped phason branch in incommensurate k2seo4. *Solid State Commun.* **48** (1983).
10. Bryan, L., Matthew S. and Fu *et al.* Nonlinear propagating modes beyond the phonons in fluorite-structured crystals. *Commun. Phys.* **3** (2020).

11. Shulumba, N., Hellman, O. & Minnich, A. J. Intrinsic localized mode and low thermal conductivity of pbse. *Phys. Rev. B* **95** (2017).
12. Manley, M. E., Abernathy, D. L., Agladze, N. I. & Sievers, A. J. Symmetry-breaking dynamical pattern and localization observed in the equilibrium vibrational spectrum of nai. *Sci. Reports* **1** (2011).
13. Manley, M. E. *et al.* Multiple high temperature transitions driven by dynamical structures in nai. *Phys. Rev. B* **89** (2014).
14. Visoly-Fisher, I., Cohen, S., Gartsman, K., Ruzin, A. & Cahen, D. Understanding the beneficial role of grain boundaries in polycrystalline solar cells from single-grain-boundary scanning probe microscopy. *Adv. Funct. Mater.* **16**, DOI: <https://doi.org/10.1002/adfm.200500396> (2006).
15. Klingshirn, C. *Optical Properties of Phonons* (Springer Berlin Heidelberg, 2007).
16. Haug, H. & Koch, S. W. *Quantum Theory of the Optical and Electronic Properties of Semiconductors* (WORLD SCIENTIFIC, 2009), 5th edn.
17. Togo, A. & Tanaka, I. First principles phonon calculations in materials science. *Scripta Materialia* **108** (2015).
18. Togo, A., Chaput, L. & Tanaka, I. Distributions of phonon lifetimes in brillouin zones. *Phys. Rev. B* **91** (2015).
19. Brorsson, J., Hashemi, A., Fan, Z. & Fransson. Efficient calculation of the lattice thermal conductivity by atomistic simulations with ab initio accuracy. *Adv. Theory Simulations* **5** (2022).
20. Bloch, P. Projector augmented-wave method. *Phys. Rev. B* **50** (1994).
21. Mortensen, J., Hansen, L. & Jacobsen, K. Real-space grid implementation of the projector augmented wave method. *Phys.Rev.B* **71** (2005).
22. Kohn, W. & Sham, L. Self-consistent equations including exchange and correlation effects. *Phys. Rev.* **140** (1965).
23. Enkovaara, J. *et al.* Electronic structure calculations with gpaw: a real-space implementation of the projector augmented-wave method. *J. Phys. Condens. Matter* **22** (2010).
24. Shukla, V., Jiao, Y., Frostenson, C. M. & Hyldgaard, P. vdw-df-ahcx: a range-separated van der waals density functional hybrid. *J. Physics: Condens. Matter* **34** (2021).
25. Eriksson, F., Fransson, E. & Erhart, P. The hiphive package for the extraction of high-order force constants by machine learning. *Adv. Theory Simulations* **2** (2019).
26. Chaput, L. Direct solution to the linearized phonon boltzmann equation. *Phys. Rev. Lett.* **110** (2013).
27. Biswas, K. *et al.* High thermoelectric figure of merit in nanostructured p-type pbte–mte (m = ca, ba). *Energy Environ. Sci.* **4** (2011).
28. Lo, S.-H., He, J., Biswas, K., Kanatzidis, M. G. & Dravid, V. P. Phonon scattering and thermal conductivity in p-type nanostructured pbte-bate bulk thermoelectric materials. *Adv. Funct. Mater.* **22** (2012).
29. Kelemen, F., Néda, A., Niculescu, D. & Cruceanu, E. On the thermal conductivity of cdte and some cdte1-xsx and cdte1-xsex solid solutions. *physica status solidi (b)* **21**, DOI: <https://doi.org/10.1002/pssb.19670210213> (1967).
30. Su, H. *et al.* Snte thermoelectric materials with low lattice thermal conductivity synthesized by a self-propagating method under a high-gravity field. *Phys. Chem. Chem. Phys.* **24** (2022).